RSC Advances

PAPER

View Article Online
View Journal | View Issue

Check for updates

Cite this: *RSC Adv.*, 2024, **14**, 10244

Synthesis, characterization, and biomedical evaluation of ethylene-bridged tetra-NHC Pd(II), Pt(II) and Au(III) complexes, with apoptosis-inducing properties in cisplatin-resistant neuroblastoma cells†

Wolfgang R. E. Büchele, ‡[a] Tim P. Schlachta, ‡[a] Andreas L. Gebendorfer,[a] Jenny Pamperin,[cd] Leon F. Richter,[a] Michael J. Sauer,[a] Aram Prokop*[bcd] and Fritz E. Kühn *[a]

Received 16th February 2024
Accepted 14th March 2024

DOI: 10.1039/d4ra01195c

rsc.li/rsc-advances

Synthesis and characterization of the first two cyclic ethylene-bridged tetradentate NHC ligands, with an unsaturated (imidazole) and saturated backbone (2-imidazoline), are described. Complexes of both ligands containing palladium(II) have been obtained. For platinum(II) and gold(III), only the unsaturated tetracarbene complexes could be isolated. The attempts to synthesize a methylene-bridged 2-imidazoline macrocycle are also described. Furthermore, a novel bisimidazolinium ligand precursor and its open-chain Pd^{II} and Pt^{II} tetracarbene complexes are obtained. Finally, it is shown that the unsaturated gold(III) tetracarbene is able to induce apoptosis in malignant SK-N-AS neuroblastoma cells *via* the mitochondrial and ROS pathway and overcomes resistance to cisplatin *in vitro*.

Open Access Article. Published on 27 March 2024. Downloaded on 4/30/2026 5:07:08 AM.
This article is licensed under a Creative Commons Attribution 3.0 Unported Licence.

Introduction

N-heterocyclic carbenes (NHCs), first described in 1991,[1] have found many applications.[2] There are several structural features that allow the tuning of their electronic properties. Ring size, the adjacent heteroatoms, *N*-substituents, and the backbone can be modified. Changing one or more structural properties of a NHC ligand can lead to significantly different reactivities and stabilities of the resulting complexes.[3] Often several NHC units are combined in multidentate ligands, making use of the chelating effect, and a plethora of multidentate NHC metal complexes has been reported.[4,5]

Our group has developed several bidentate and cyclic tetradentate NHC ligands. The respective transition metal complexes have been applied *e.g.* in medicinal chemistry[6,7] and epoxidation catalysis.[3] While the bidentate ligands can form open-chain tetracarbene complexes,[8,9] the tetradentate ligands give cyclic tetracarbene compounds. Most commonly applied in our recent examinations is the calix[4]imidazolium ligand precursor (**a**, Fig. 1).[10] Its iron complex (**c**) can be used as olefin epoxidation catalyst achieving unprecedented activity.[3] Coinage metal tetracarbene complexes (and metal NHC complexes in general[11–17]) have been investigated regarding their antiproliferative activity and selectivity against cancer cells (**b**, **d–f**, Fig. 1).[6,7]

[a]*Technical University of Munich, School of Natural Sciences, Department of Chemistry and Catalysis Research Center, Molecular Catalysis, Lichtenbergstraße 4, 85748 Garching, Germany. E-mail: fritz.kuehn@ch.tum.de; Tel: +49 89 289 13477*

[b]*Department of Pediatric Hematology/Oncology, Children's Hospital Cologne, Amsterdamer Straße 59, 50735 Cologne, Germany*

[c]*Department of Pediatric Oncology/Hematology, Helios Clinics Schwerin, Wismarsche Straße 393-397, 19055 Schwerin, Germany. E-mail: aram.prokop@helios-gesundheit.de*

[d]*Department of Human Medicine, MSH Medical School Hamburg, Am Kaiserkai 1, 20457 Hamburg, Germany*

† Electronic supplementary information (ESI) available: Synthetic details, biological studies, analytical data and crystallographic data. CCDC 2299372–2299374. For ESI and crystallographic data in CIF or other electronic format see DOI: https://doi.org/10.1039/d4ra01195c

‡ These authors contributed equally to this work.

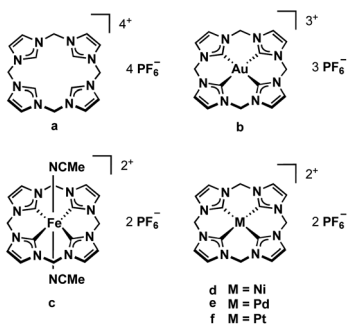

Fig. 1 Tetracarbene ligand precursor **a** and derived transition metal complexes **b–f**.

© 2024 The Author(s). Published by the Royal Society of Chemistry

Open Access Article. Published on 27 March 2024. Downloaded on 4/30/2026 5:07:08 AM.
This article is licensed under a Creative Commons Attribution 3.0 Unported Licence.

In this study, the scope of multidentate NHC ligands is extended with an ethylene-bridged bisimidazolinium ligand precursor and two cyclic ethylene-bridged tetradentate NHC ligands, with an unsaturated (imidazole) and saturated backbone (2-imidazoline). Pd^{II}, Pt^{II} and Au^{III} tetracarbene complexes containing the novel ligands are synthesized, characterized and applied in preliminary medicinal studies regarding their activity in inducing apoptosis in malignant cells. Finally, the synthetic attempts to a calix[4]imidazolinium macrocycle (structurally analog to **c** but with a saturated backbone) are described, because there is an increasing demand for reliable training data, including data on negative outcomes, for machine learning systems in chemistry.[18]

Especially the two new macrocyclic ligand precursors are intended to lay the foundation for electronic comparisons induced by the different backbone in future studies. The unsaturated backbone of the imidazole moiety causes partial aromaticity, increasing NHC stability by *ca.* 100 kJ mol^{-1}.[19–21] A saturated backbone, in turn, can lead to higher basicity because the electron density is more concentrated on the C2 carbene carbon atom due to the lack of π-interactions.[22]

Results and discussion

The synthesis of a saturated macrocyclic ligand precursor similar to **c**, but containing 2-imidazoline moieties instead of imidazole, calix[4]imidazolinium, was pursued parallel to the synthesis of the other ligand precursors. However, the synthesis was not successful with the chosen synthetic approaches as described in the ESI.†

Synthesis and characterization of H_2L3

H_2L3 is based on the literature known ethylene-bridged imidazoline moiety (**1**).[23] Alkylation of **1** with MeI in MeCN at 82 °C, followed by an anion exchange with NH_4PF_6 in water, gives **H_2L3** in 91% yield (Fig. 2).

Synthesis and characterization of $H_4L5/6$ and $H_4L8/L9$

For the preparation of **$H_4L5/6$** and **$H_4L8/9$**, a slightly modified literature procedure for similar macrocycles was used (Fig. 3).[10] Ring closure to form the macrocyclic imidazolium salt **a** is commonly achieved with $CH_2(OTf)_2$,[3] but also CH_2Br_2 is reported.[24] Here the ethylene-bridged imidazoline **1** (ref. 23) and the ethylene-bridged imidazole **7** (ref. 25) are reacted with ethylene bistriflate (**4**) under dry conditions at −45 °C over a period of 5 h in dry MeCN for **H_4L5** and **H_4L8** (see ESI†).

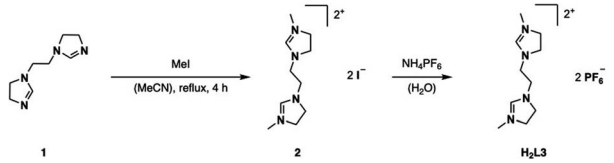

Fig. 2 Synthesis of ligand precursor H_2L3 *via* alkylation and anion exchange.

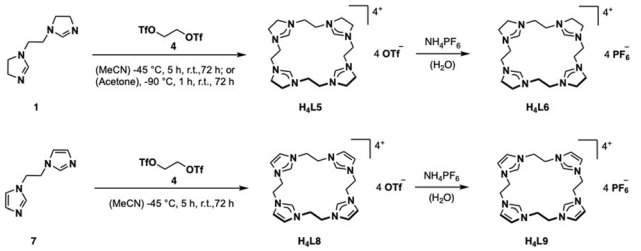

Fig. 3 Synthesis of ligand precursors $H_4L5/6$ and $H_4L8/9$ *via* ring closure with ethylene bistriflate and anion exchange.

The synthesis of **H_4L5** and **H_4L8** yields a mixture of a 20-membered macrocycle (87% **H_4L5** and 90% **H_4L8**, as determined by NMR), consisting of four imidazole (C[4]) units, and a 30-membered macrocycle (13% **H_4L5**, 10% **H_4L8**) consisting of six imidazole (C[6]) units (see ESI†). Separation attempts of C[4] and C[6] *via* column chromatography, precipitation or sublimation were not successful. However, by increasing the cooling period during the addition of the ethylene bistriflate at −45 °C to a total of 5 h, the purity of the kinetically preferred C[4] unit could be easily increased up to 98% C[4] for **H_4L5** and in case of **H_4L8** an increase up to 100% (ESI†). Due to the absence of similar macrocyclic imidazolinium compounds, **H_4L5** is compared to **a** and **H_4L8** in the following.[3]

Relative to **a**, all signals of **H_4L5** and **H_4L8** are upfield shifted, indicating a higher electronic density due to the +I effect of the ethylene bridge leading to an increased shielding effect in the NMR.[10,26] The higher upfield shift of **H_4L5** compared to **H_4L8** can be explained by the electronic inducing effect of the saturated bond.[20,26,27]

Unlike in ^{1}H-NMR, each individual ^{13}C signal of **H_4L8** in DMSO-d_6 is in the same range as the signals obtained for the macrocyclic compound **a**.[10] However, in case of **H_4L5**, opposite to the ^{1}H-NMR, the C2 carbon resonance at 159.16 ppm is downfield shifted compared to **H_4L8** and **a** (**H_4L8**, $\Delta\delta \leq$ 22.08 ppm, **a**, $\Delta\delta \leq$ 22.0 ppm), thus contradicting expectations. According to literature and as described by H. V. Huynh, the hypothetical free carbene of the imidazoline ligand **H_4L5** should be a stronger σ-donor than **H_4L8**, so an enhanced upfield shift of the C2 signal of **H_4L5** should have been detectable.[20,28,29] Interestingly this expectation is not met here, and apparently other factors play a role. Every other resonance in the ^{13}C-NMR is upfield shifted.[10]

Salt metathesis of the formed macrocyclic salts can be performed with NH_4PF_6 to increase the solubility in organic solvents and as additional purification step.[3,30] Thus, an anion exchange in water towards PF_6^- is conducted with **H_4L5** and **H_4L8**, resulting in **H_4L6** (81%) and **H_4L9** (88%).

Synthesis and characterization of complexes (Pd/PtL3, PdL5/6, Pd/PtL8, Pd/AuL9)

A well-established route to obtain NHC complexes is to convert the corresponding imidazolium salts with group 10 metal acetates. In this reaction, the acetate serves as an internal base capable of deprotonating imidazolium- and imidazolinium

Open Access Article. Published on 27 March 2024. Downloaded on 4/30/2026 5:07:08 AM.
This article is licensed under a Creative Commons Attribution 3.0 Unported Licence.

salts to form NHCs, which subsequently coordinate to the metal.[6,31–33] An alternative route is *via* a silver transmetalation.[34] In the first approaches, attempts were made to synthesize the respective Ag^{I} complex with **H_2L3** to obtain a dinuclear structure similar to already published open chain bis-NHC-complexes.[9,25,35] However, no product formation was observed in our case. Either no reaction took place or complex signals were observed in the aliphatic region of $\delta = 1.9$–4.4 ppm in the ^{1}H-NMR after purification, indicating the decomposition of **H_2L3**. Several other conditions with different Ag^{I}-salts and addition of sodium acetate as internal base at different temperatures were tested without success. A possible problem might be the stability of the Ag^{I}-complex. Another issue might be hydrolysis of imidazolines under acidic and basic conditions.[36,37] It has been proposed in literature that the moisture in the solvent can react with sodium acetate to generate hydroxide ions which can attack the electrophilic center of the C2 carbon and lead to ring-opening products, rather than nucleophilic attacking the acidic proton at the C2 carbon.[38] Therefore, the next attempts were conducted under moisture-free reaction conditions by using dried solvents. Even the direct metalation with palladium(II) acetate or palladium(II) chloride under dry reaction conditions did not lead to the desired product. The focus was then shifted to a combination of the transmetalation route using Ag_2O *in situ* with the direct metalation, by applying the respective metal precursor and sodium acetate as a mild base in dry solvents (Fig. 4).

The absence of the acidic imidazolinium proton signal and appearance of characteristic carbene carbon signals confirms the successful formation of **PdL3** and **PtL3**. Unfortunately, despite several attempts, a clean elemental analysis for **PtL3** could not be obtained. Also, the ^{1}H-NMR of **PtL3** shows some impurities, which could not be identified and no ^{195}Pt isotope coupling phenomena was observed in the ^{13}C-NMR.

The carbene carbon signal of **PdL3** at 194.29 ppm in DMSO-d_6 [**PtL3**; 188.38 ppm in CD_3CN], is surprisingly downfield shifted compared to other Pd(II) bis-NHCs reported in literature.[39,40] Due to the theoretically stronger σ-donation of the imidazolinylidene ligand **H_2L3** compared to its unsaturated analog, an upfield shift of the $^{13}C_{NHC}$ signal was expected. Literature indicates that the significant downfield shift of the carbene carbon resonance from imidazolium to imidazolinium compounds is a general phenomenon.[38,41,42] Another interesting fact is that the analytic data, including HR-ESI-MS and elemental analysis, are not supporting a dinuclear complex or a mono-carbene complex as expected, but indicate that **PdL3** has rather a $[\mathbf{Pd(L3)_2}](PF_6)_2$ structure similar to **e**. This is further

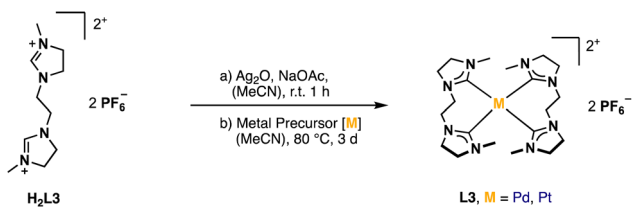

Fig. 4 General synthesis of **Pd/PtL3**.

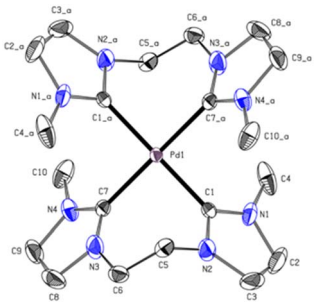

Fig. 5 ORTEP-style representation of the cationic fragment of complex **PdL3**. Hydrogen atoms and hexafluorophosphate anions are omitted for clarity. Thermal ellipsoids are shown at a 50% probability level. Selected bond lengths (Å) and angles (°): C1–Pd1 2.039(2); C7–Pd1 2.038(2); C7_a–Pd1–C7 180.0; C7–Pd1–C1_a 91.64(9); C7–Pd1–C1 88.36(9), C7_a–Pd1–C1_a–N2_a 55.30.

confirmed by single-crystal X-ray diffraction (SC-XRD). The **PdL3** complex displays a distorted square planar structure. Two **L3** ligands coordinate to the Pd center, resulting in an open-chain tetracarbene complex of similar geometry like the cyclic complex **e**.[34] The Pd–C (2.039 Å, 2.038 Å) distances are in good accord with palladium(II) NHC complexes reported in literature.[34,39] The alkyl groups of the ligand **L3** adopt a *syn* conformation in the solid state, while the imidazole rings are tilted by 55.30° out of the palladium square plane (Fig. 5).

The **PtL3** complex exhibits a similarly distorted square planar structure compared to **PdL3**. The Pt–C (2.033 Å, 2.039 Å) distances are comparable to similar literature known group 10 NHC compounds.[43–47] The alkyl groups of **L3** also adopt a *syn* conformation, while the imidazole rings are tilted by 50.53° out of the palladium square plane as in **PdL3** (Fig. 6).

Complex PdL5/6 and PdL8/9

Since **H_4L5** and **H_4L8** are quite similar to other macrocycles (**a**), it seemed suitable to synthesize **PdL5** and **PdL8** according to alike compounds *via* the direct metalation route.[32] Therefore, **H_4L8** was first converted with $Pd(OAc)_2$ in a mixture of dry

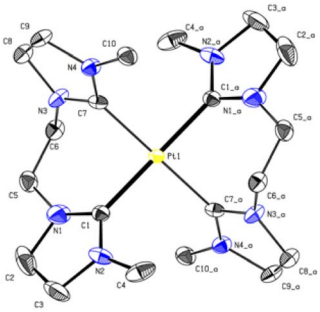

Fig. 6 ORTEP-style representation of the cationic fragment of complex **PtL3**. Hydrogen atoms and hexafluorophosphate anions are omitted for clarity. Thermal ellipsoids are shown at a 50% probability level. Selected bond lengths (Å) and angles (°): Pt1–C1 2.0337 (18); Pt1–C7 2.039 (6), C1_a–Pt1–C1 180.00(7); C1–Pt1–C7_a 91.2(5); C1–Pt1–C7 88.8(5), C7_a–Pd1–C1_a–N2_a 50.53°.

© 2024 The Author(s). Published by the Royal Society of Chemistry

Open Access Article. Published on 27 March 2024. Downloaded on 4/30/2026 5:07:08 AM.
This article is licensed under a Creative Commons Attribution 3.0 Unported Licence.

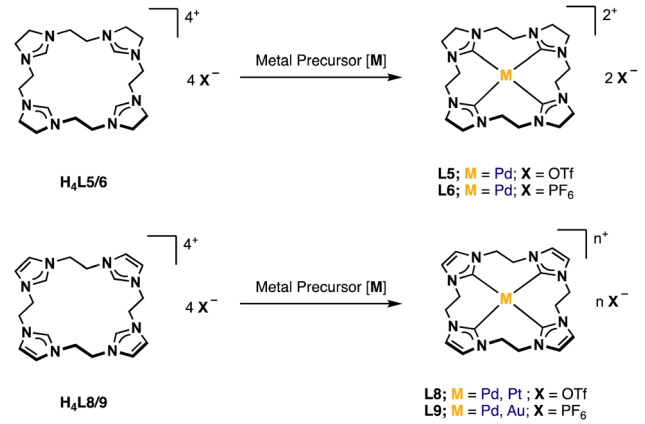

Fig. 7 General synthesis of PdL5/6, Pd/PtL8 and Pd/AuL9.

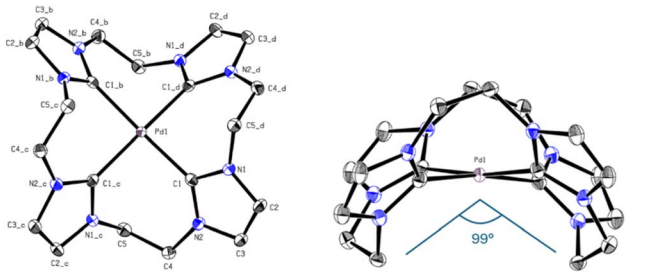

Fig. 8 ORTEP-style representation of the cationic fragment of complex PdL9. Hydrogen atoms and hexafluorophosphate anions are omitted for clarity. Thermal ellipsoids are shown at a 50% probability level. Selected bond lengths (Å) and angles (°): C1–Pd 2.019(2), C1–Pd1–C1_b 172.03(12), C1–Pd1–C1_d–N2_d 53.62, C5–Pd1–C5_b 98.97°.

DMSO/MeCN (1 : 1) at 40 °C for 16 h.[34] However, no product formation was observed after work-up. Several other conditions such as increasing temperature and reaction time led to the absence of the imidazolium protons and the formation of new product signals in the ^{1}H-NMR after 4 d at 80 °C. Still these intensities were very low, and no product could be isolated. Another approach was tried *via* the transmetalation route with Ag^I salts, but this also led to no product formation. Finally, both **PdL8** (50%, Fig. 7) and **PdL5** (3%) could be obtained by applying the same reaction conditions as for the already synthesized complexes **PdL3** and **PtL3**. The yield of the imidazolinylidene tetracarbene complex could be increased to 46%, by using **H_4L6** instead of **H_4L5**, resulting in **PdL6**.

Again, the absence of the acidic position 2 proton signals in the ^{1}H-NMR and appearance of the carbene carbon peaks confirm the formation of Pd(II) carbene complexes. The observed chemical shift of **PdL8** is in the typical range of Pd(II) tetra-NHC compounds and indicates the formation of a complex with similar coordination sphere as **e**.[6,34,45] The ^{1}H-NMR of **PdL5** in CD_3CN shows three signals, with two of them in a similar range to **PdL8** and one upfield shifted signal of the backbone protons. As already mentioned in the discussion of **H_4L5**, the ^{13}C-NMR of **PdL5** is contrary to expectations. The carbene carbon of **PdL5** (191.30 ppm) is surprisingly strong downfield shifted compared to **PdL8** (165.84 ppm) and in a similar range to the carbene carbon of **PdL3** (195.6 ppm in CD_3CN). Literature indicates that the significant downfield shift of the carbene carbon resonance from imidazole to imidazoline compounds is a general phenomenon.[38,41,42] The uncertainty of a ^{13}C-NMR measurement is expected to be below 0.1 ppm; by using three times the weighted standard deviation, a difference of >0.4 ppm is required for a significant difference that exceeds the statistic uncertainty.[3,48] Therefore, **PdL5** (191.30 ppm in CD_3CN) and **PdL8** (165.84 ppm in CD_3CN) show a sufficiently different chemical shift to allow its discussion. In general, the normal NHC unit (without any modification) of the tetracarbene ligands is in a range of rather low to negligible π-backdonation, hence the changes in electronic properties are dominated by the σ-donation of the tetracarbenes.[3,29] According to literature, the imidazoline ligand **L5** should be in general a stronger σ-donor than **L8**, so an enhanced upfield shift of the carbene signal would have been detectable.[3,20,28,29] Interestingly, this expectation is also not met here, and apparently other factors may play a role, as already observed with **PdL3** and **PtL3**. Therefore, further investigations on this subject, *e.g.* by means of DFT calculations, have to be carried out, since only conjectures can be made with the present analytical data. The elemental analysis and HR-ESI-MS for **PdL8** are in accord with a composition **[Pd(L8)]**$(OTf)_2$ similar to **e**. It needs to be noted that no clean elemental analysis of **PdL6** could be obtained. However, the elemental analysis and HR-ESI-MS of **PdL6** are in accordance with the composition **[PdL6]**$(PF_6)_2$. Due to unsatisfying results in crystallization of **PdL8**, an anion exchange in water towards PF_6^- was conducted, resulting in **PdL9** (41%). Single crystals suitable for SC-XRD were obtained by slow diffusion of Et_2O into MeCN solution of **PdL9**. As expected, the Pd(II) ion is coordinated in a nearly square planar fashion with C–Pd–C angles deviating from 180° by ~8°, thus lifting the metal slightly above the carbene carbon atom plane (Fig. 8). However, due to the C_2-bridge, the ligand is strongly bent (C5–Pd1–C5_b = 98.97°) and adopts a crisp-shape, while tilting the imidazole rings 53.62° in an alternating pattern out of the palladium square plane.[49] The Pd–C distance (2.019 Å) is comparable to those of other cyclic Pd(II) tetracarbene compounds reported in literature.[6,34,43,45–47]

In the following Table 1 the M–$C_{carbene}$ bond lengths [Å], the $C_{carbene}$–M–$C_{carbene}$ angle [°], the tilt of the NCN unit [°] of the complexes **Pd/PtL3** and **PdL9** and additionally the C_{bridge}–M–C_{bridge} angle [°] for **PdL9** are summarized.

Table 1 Summary of the M–$C_{carbene}$ bond lengths [Å], the $C_{carbene}$–M–$C_{carbene}$ angle [°], the tilt of the NCN unit [°] of the complexes Pd/PtL3 and PdL9 and the C_{bridge}–M–C_{bridge} angle [°] for PdL9

Compound	PdL3	PtL3	PdL9
M–$C_{carbene}$ [Å]	2.038|2.039	2.033|2.039	2.019
$C_{carbene}$–M–$C_{carbene}$ [°]	180	180	172.03
Tilt NCN unit [°]	55.30	50.53	53.62
C_{bridge}–M–C_{bridge} [°]	—	—	98.97

Open Access Article. Published on 27 March 2024. Downloaded on 4/30/2026 5:07:08 AM.
This article is licensed under a Creative Commons Attribution 3.0 Unported Licence.

Complex PtL8

Applying the same reaction conditions and work-up methods to $Pt(MeCN)_2Cl_2$ instead of $Pd(OAc)_2$ results in the formation of **PtL8** (25%,Fig. 7). The absence of acidic proton signals in the ^{1}H-NMR and the appearance of the carbene ^{13}C-peak at 159.39 ppm in CD_3CN confirms the formation of the respective Pt(II) complex. The chemical shift of the carbene carbon is in accordance with Pt(II) tetra-NHC complexes previously reported in literature and is slightly shifted to the upfield compared to **PdL8** ($^{13}C_{NHC}$ in CD_3CN at 165.84 ppm) by 6.45 ppm.[43,46,50] No ^{195}Pt isotope coupling was observed. The ^{1}H-NMR in CD_3CN shows similar signals compared to **PdL8**, where the bridge protons also split into two multiplets at 5.01 and 4.44 ppm. In addition, HR-ESI-MS is in accordance to a similar composition as **PdL8**. Despite multiple attempts, no single crystals suitable for SC-XRD were obtained. However, the discussed analytical data strongly support a similar structure compared to **PdL8** and similarly structured tetracarbene ligand.[6,34]

Complex AuL9

For the synthesis of **AuL9** (Fig. 7), the same reaction conditions were applied as reported in the literature for similar complexes.[51] Therefore, **H_4L8** was converted with $KAuCl_4$ and NaOAc in dry DMSO under exclusion of light at 100 °C for 5 h. After the work-up, including an ion exchange to PF_6^- as a purification step, **AuL9** (47%) was obtained. The absence of acidic proton signals in the ^{1}H-NMR and the appearance of a new ^{13}C-peak at 146.03 ppm in CD_3CN confirm the formation of the respective Au(III) complex. The chemical shift of the carbene carbon is in accord with Au(III) tetracarbene complex (**e**) previously reported in literature and slightly downfield shifted by 1.79 ppm when compared to **e**.[51] Furthermore, the backbone carbons are also slightly downfield shifted by 0.68 ppm. The ^{1}H-NMR in CD_3CN shows similar signals compared to complex **PdL8** and **PtL8** with the backbone protons at 7.47 ppm and the bridge protons as two multiplets in close proximity at 4.83 and 4.71 ppm. Both elemental analysis[52] and HR-ESI-MS are in agreement with the composition **[Au(L15)]**$(PF_6)_3$. Although no single crystals suitable for SC-XRD were obtained, the discussed analytical data strongly support the coordination of one tetracarbene ligand similar to **PdL9**.

Biological evaluation

Induction of apoptosis as cell death type

PdL3, **PdL8**, **AuL9** and their respective protonated ligand precursors were tested for their apoptotic effects on Nalm-6 cells (human B cell precursor leukemia cell line) and SK-N-AS cells (human neuroblastoma cell line) at different concentrations and quantified by the nuclear DNA fragmentation by flow cytometry analysis. **PdL3** and **PdL8** as well as the ligand precursors do not show any apoptosis inducing effects in Nalm-6 cells and SK-N-AS cells (see ESI†). **AuL9** shows no apoptotic effect in Nalm-6 cells, but significant apoptosis induction by **AuL9** is detected in SK-N-AS cells (Fig. 9A); therefore, the effect of **AuL9** in SK-N-AS cells was further characterized.

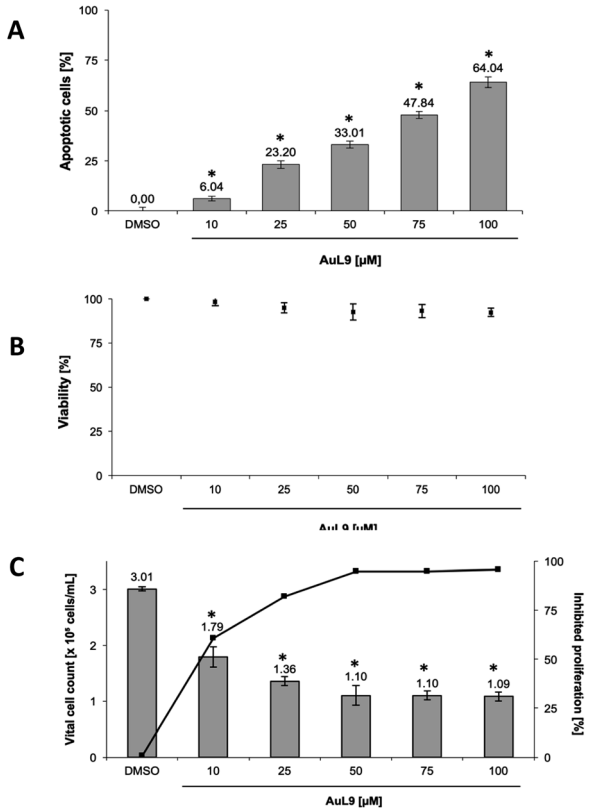

Fig. 9 (A) **AuL9** induces apoptosis in SK-N-AS cells. The cells were treated with different concentrations of **AuL9** and incubated for 96 h. Nuclear DNA fragmentation was analyzed. (B) To exclude unspecific cytotoxic effects, such as necrotic cell death, the viability of SK-N-AS cells was determined by measurement of LDH release into the medium after 2 h of incubation with different concentrations of **AuL9**. No significant LDH release could be detected in cells treated with **AuL9** up to a concentration of 100 µM. Values are given as mean% of DMSO control ± SD ($n = 3$). (C) The inhibition of proliferation of **AuL9** treated SK-N-AS cells was measured after 48 h using the CASY Cell-Counter System. A significant inhibition of cell growth was observed at concentrations as low as 10 µM. Inhibition of proliferation is given in mean% of control ± SD ($n = 3$); *: $p < 0.05$ *vs.* DMSO, *t*-test.

To exclude necrotic effects of **AuL9**, lactate dehydrogenase (LDH) leakage from SK-N-AS cells after 2 h incubation with **AuL9** was measured. LDH is released from the cell in case of necrosis and can be detected in the cell culture medium in case of loss of cell integrity and thus serves as a necrosis indicator.[53] **AuL9** shows no significant non-specific cytotoxic effects on SK-N-AS cells in the relevant concentration range up to 100 µM (Fig. 9B).

In addition to apoptosis induction, it was tested whether **AuL9** can inhibit the proliferation of malignant cells. For this purpose, SK-N-AS cells were incubated with different concentrations of **AuL9** for 48 hours. The proliferation inhibition was determined by comparing the total cell number of vital cells of the DMSO control with the total cell number of vital cells of the treated cells. The results show that **AuL9** inhibits cell proliferation of SK-N-AS cells in a dose-dependent manner (Fig. 9C). A concentration of 50 µM **AuL9** causes nearly 100% inhibition of proliferation, indicating G1 arrest.

© 2024 The Author(s). Published by the Royal Society of Chemistry

Open Access Article. Published on 27 March 2024. Downloaded on 4/30/2026 5:07:08 AM.
This article is licensed under a Creative Commons Attribution 3.0 Unported Licence.

For the investigation of the mechanism of action of **AuL9**, the mitochondrial membrane potential of SK-N-AS cells was measured after 48 h incubation with **AuL9**. It was shown that the mitochondrion and thus the intrinsic apoptosis pathway plays at least a partial role in the effect of **AuL9** (Fig. 10A).

To further characterize the role of mitochondria in **AuL9**-induced apoptosis, the apoptosis pathway mediated by reactive oxygen species (ROS) was investigated. Therefore, *N*-acetylcysteine (NAC) as a known ROS inhibitor and H_2O_2, which belongs to the ROS, as a positive control was investigated. It was shown that apoptosis induction could be significantly inhibited by NAC. It can therefore be concluded that the generation of ROS plays a role in the **AuL9**-induced apoptosis (Fig. 10B). However, it is not possible in the present state to be sure how the ROS are generated and whether **AuL9** directly leads to an increased ROS production or triggers pathways that result in the generation of ROS.

Overcoming cisplatin resistance

Cisplatin is a well-known chemotherapeutic agent for the treatment of many different types of cancer.[54] The development of resistance in tumor cells is a major problem in therapy and is usually the limiting factor in the cure of cancer patients.[55]

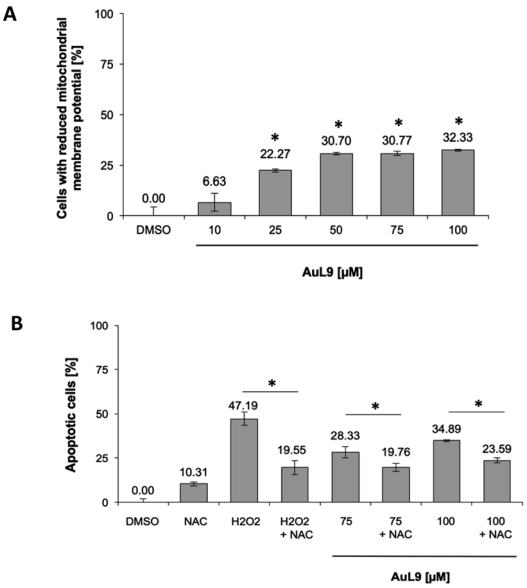

Fig. 10 (A) The mitochondrial membrane potential in SK-N-AS cells was impaired by **AuL15** treatment, which implicates mitochondrial pathway involvement in apoptosis induction. The mitochondrial membrane potential was measured by flow cytometric analysis in SK-N-AS cells after 48 h of incubation with different concentrations of **AuL15** and staining with the cationic dye JC-1. Values are mean% of cells with low mitochondrial membrane potential ± SD ($n = 3$); *: $p < 0.05$ *vs.* DMSO, *t*-test. **B** The induction of apoptosis in SK-N-AS cells in response to **AuL15** treatment was shown to be dependent on the ROS mediated pathway. The cells were incubated for 72 h with 50 µM H_2O_2 as a positive control or different concentrations of **AuL15** with or without pretreatment of the cells with the ROS inhibitor *N*-acetylcysteine (NAC, 5 mM) 1.5 h prior to substance addition. Nuclear DNA fragmentation was analyzed by flow cytometric analysis. Values are mean% of apoptotic cells ± SD ($n = 3$); *: $p < 0.05$ *vs.* DMSO, *t*-test.

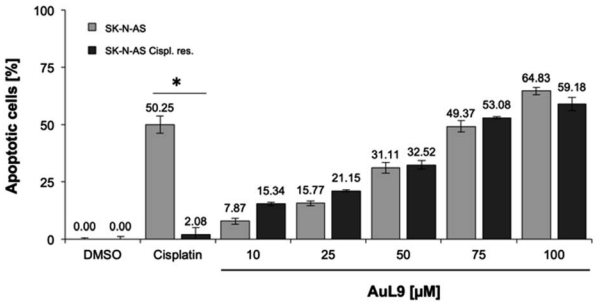

Fig. 11 SK-N-AS and SK-N-AS cisplatin resistant cells were treated with different concentrations of **AuL15** and incubated for 96 h. It is shown that **AuL9** was also effective in inducing apoptosis in cisplatin resistant cells, thus overcoming resistance. 8.25 µM cisplatin has been used as a positive control to prove resistance. Nuclear DNA fragmentation was analyzed by flow cytometric analysis. Values are mean% of apoptotic cells ± SD ($n = 3$); *: $p < 0.05$ *vs.* DMSO, *t*-test.

Therefore, it is of great importance for drug development that new agents are able to overcome cytostatic drug resistance. In addition to SK-N-AS cells, **AuL9** was tested on cisplatin resistant SK-N-AS cells and cisplatin resistance overcoming could be demonstrated (Fig. 11). In a previous characterization of the cisplatin resistant SK-N-AS cells, procaspase-8 under expression was shown.[56] The cisplatin resistance overcoming of SK-N-AS cells indicates that procaspase-8 has a minor role in **AuL9**-induced apoptosis.

Conclusion and outlook

A synthetic approach to a calix[4]imidazolinium macrocycle as saturated analog to **a** is presented. The synthesis of two new macrocyclic ligand systems, being bridged by ethylene groups and containing imidazoline (**H_4L5/6**) and imidazole moieties (**H_4L8/9**) are discussed. In addition, a novel bisimidazolinium ligand precursor (**H_2L3**) is described. All complexes (**Pd/PtL3**, **PdL5/6**, **Pd/PtL8**, **Au/PdL9**) with their respective ligands synthesized in this work are not accessible *via* the direct metalation of the respective ligand, due to irreproducible or unreliable results, except for **AuL9**. Even the route *via* the silver salt transmetalation does not lead to reliable results. The silver complexes of the respective ligands could not be isolated, probably due to instability of the respective complexes. Therefore, a modified synthetic method has been established. Here, *in situ* transmetalation with silver oxide is used in combination with the metal precursor and an excess of sodium acetate as a mild base, resulting in the corresponding complexes. Furthermore, the complexes **PdL3**, **PdL8**, **AuL9** and their respective ligands were tested for their ability to induce apoptosis on Naml-6 and SK-N-AS cells. According to the experiments performed, the data suggest that **AuL9** is capable of inducing apoptosis in malignant cells *via* the mitochondrial and ROS pathway. However, so far, an effect could only be observed on SK-N-AS neuroblastoma cells. In addition, a relatively high dose of **AuL9** is required to induce apoptosis in neuroblastoma cells, which could be challenging for clinical applicability. **AuL9** is able to overcome resistance to cisplatin in

Open Access Article. Published on 27 March 2024. Downloaded on 4/30/2026 5:07:08 AM. This article is licensed under a Creative Commons Attribution 3.0 Unported Licence.

neuroblastoma cells (SK-N-AS) *in vitro*. Further characterization experiments would be required to determine the exact mechanism of action of **AuL9**, for example identification of molecular targets that are involved in the **AuL9** induced apoptosis, as well as the selectivity for cancer cells.

Experimental section

General procedures and analytical methods

Unless otherwise stated, all manipulations were performed under normal atmosphere without dried and degassed chemicals. All syntheses regarding the complexes were conducted under the exclusion of light. Every work-up was performed under normal atmosphere without dried and degassed chemicals; the complexes' work-ups were conducted in addition under the exclusion of light unless otherwise stated. Purification, in case of the Pt and Pd complexes, is achieved by dissolving the crude product in MeCN and filtering it through basic aluminum oxide to remove impurities. Acidic aluminum oxide promotes the decomposition of the complexes while pH-neutral aluminum oxide leads in smaller yields.[6] All obtained complexes are air- and water stable; however, **PtL3**, **PtL8** and **AuL9** decompose after extensive exposition to light. Solvents were obtained water-free from a MBraun solvent purification system and stored over molecular sieves (3 Å). The procedures for novel compounds obtained during the synthetic approaches to the saturated macrocyclic ligand precursor, containing 2-imidazoline moieties instead of imidazole, calix[4]imidazolinium, (2-imidazoline, *N*-benzyl-2-imidazoline, 3,3′-methylenebis(1-benzyl-2-imidazolinium)dibromide, N^1,N^1,N^2,N^2-tetrabenzylethane-1,2-diamine, *tert*-butyl (2-aminoethyl)carbamate, *tert*-butyl 2-imidazoline-1-carboxylate) are stated in the ESI.† *N*-Benzylethylenediamine (**12**),[57–59] ethylenebis(trifluoromethanesulfonate) (**4**),[60] 1,1′-ethylene-di-2-imidazoline (**1**)[23] and 1,1′-ethylenebis-1*H*-imidazolyl (**7**)[25,61] were synthesized according to literature procedures. All other reagents were purchased from commercial suppliers and used without further purification. NMR spectra were recorded on a Bruker Avance DPX 400 (^{1}H-NMR, 400 MHz; ^{13}C-NMR, 100 MHz; ^{19}F-NMR, 376 MHz) and chemical shifts are given in δ values in ppm (parts per million) relative to TMS (tetramethylsilane) and reported relative to the residual signal of the deuterated solvent.[62] Elemental analysis (C/H/N) were obtained by the Microanalytical Laboratory at Technische Universität München. Electrospray ionization mass spectrometry (ESI-MS) data were acquired on a Thermo Fisher Ultimate 3000 and with higher resolution (HR-ESI-MS) on Exactive Plus Orbitrap from Thermo Fisher.

Synthetic procedures

Alkylbisimidazoline diiodide (2). **1** (5.00 g, 30.0 mmol, 1.00 eq.) is dissolved in MeCN (300 mL) and MeI (213 g, 1.50 mol, 50.0 eq.) is added. The resulting reaction mixture is heated to reflux for 4 h. After cooling to ambient temperature, all volatile compounds are removed *in vacuo*. The resulting crude material is redissolved in a small amount of MeCN (5 mL) and an off-white solid is precipitated after the addition of Et_2O (40 mL). The crude material is collected *via* centrifugation and washed with (3 × 5 mL) Et_2O. After removal of all volatile compounds *in vacuo*, **2** is obtained as an off-white solid (11.1 g, 24.7 mmol, 82%). ^{1}H-NMR (400 MHz, DMSO-d_6) δ (ppm) = 8.54 (s, 2H, N–C*H*–N), 3.91 (s, 8H, CH_3–N–CH_2–CH_2), 3.70 (s, 4H, CH_2–CH_2), 3.12 (s, 6H, CH_3). ^{13}C-NMR (101 MHz, DMSO-d_6) δ (ppm) = 159.12 (N–*C*H–N), 50.96 ($C_{(backbone)}$), 48.70 ($C_{(backbone)}$), 45.02 (*C*H_2–*C*H_2), 35.08 (*C*H_3). Elemental analysis: for $C_{10}H_{20}I_2N_4$ (%) anal. calc.: C: 26.68, H: 4.48, N: 12.45, found: C: 26.66, H: 4.48, N: 12.39.

Alkylbisimidazolinium hexafluorophosphate (H_2L3). **2** (100 mg, 222 μmol, 1.00 eq.) is dissolved in H_2O (1 mL) and added to a solution of NH_4PF_6 (217 mg, 1.33 mmol, 6.00 eq.) in H_2O (1 mL). The resulting white precipitate is collected, washed three times with H_2O (2 mL, 2 mL, 1 mL) and dried subsequently *in vacuo*. Without further purification, the titled compound **H_2L3** is obtained as a white solid (98 mg, 202 mmol, 91%). ^{1}H-NMR (400 MHz, DMSO-d_6) δ (ppm) = 8.39 (s, 2H, N–C*H*–N), 3.88 (s, 8H, CH_3–N–CH_2–CH_2), 3.67 (s, 4H, CH_2–CH_2), 3.11 (s, 6H, CH_3). ^{13}C-NMR (101 MHz, DMSO-d_6) δ (ppm) = 158.77 (N–*C*H–N), 50.36 ($C_{(backbone)}$), 48.12 ($C_{(backbone)}$), 44.55 (*C*H_2–*C*H_2), 34.43 (*C*H_3). ^{19}F-NMR (376 MHz, DMSO-d_6) δ (ppm) = −70.15 (d, $^1J_{P-F}$ = 713 Hz, PF_6^-). Elemental analysis: for $C_{10}H_{20}F_{12}N_4P_2$ (%) anal. calc.: C: 24.70, H: 4.15, N: 11.52, found: C: 24.28, H: 4.01, N: 11.17.

Calix[4](–Et–Et–)imidazoliniumtrifluoromethanesulfonate (H_4L5). **1** (1.00 g, 6.17 mmol, 2.00 eq.) is dissolved in dry MeCN (1.5 L), cooled to −45 °C and a solution of **4** (2.02 g, 6.20 mmol, 2.01 eq.) in dry MeCN (50 mL) is added dropwise over 6 h. After the addition, the reaction mixture is stirred for 72 h at ambient temperature. All volatile compounds are removed *in vacuo* and the resulting crude material is dried subsequently *in vacuo*. Without further purification the titled compound **H_4L5** is obtained as an off-white solid (1.50 g, 1.54 mmol, 50%). Note: everything is conducted under inert conditions. ^{1}H-NMR (400 MHz, DMSO-d_6) δ (ppm) = 8.46 (s, 4H, N–C*H*–N), 3.95 (s, 16H, C$H_{2(bridge/backbone)}$), 3.74 (s, 16H, C$H_{2(bridge/backbone)}$). ^{13}C-NMR (101 MHz, DMSO-d_6) δ (ppm) = 159.16 (N–*C*H–N), 120.80 (q, $^1J_{19F-13C}$ = 320 Hz, OTf^-), 48.15 (*C*$H_{2(bridge/backbone)}$), 44.54 (*C*H_2–*C*$H_{2(bridge/backbone)}$). ^{19}F-NMR (376 MHz, DMSO-d_6) δ (ppm) = −77.74 (CF_3). Elemental analysis for $C_{24}H_{36}N_8O_{12}F_{12}S_4$ (%) anal. calc.: C 29.27; H 3.68; N 11.38; S 13.02 found: C 29.37; H 3.67; N 11.01; S 13.12.

Calix[4](–Et–Et–)imidazoliniumhexafluorophosphate (H_4L6). **H_4L5** (300 mg, 304 μmol, 1.00 eq.) is dissolved in H_2O (50 mL) and added to a solution of NH_4PF_6 (223 mg, 1.37 mmol, 4.50 eq.) in H_2O (50 mL). The resulting white precipitate is collected, washed three times with H_2O (10 mL, 7 mL, 5 mL), Et_2O (3 mL, 2 mL) and dried subsequently *in vacuo*. Without further purification, the titled compound **H_4L6** is obtained as a white solid (240 mg, 248 μmol, 81%). However, a small amount of OTf^- is still detectable in the ^{19}F-NMR. ^{1}H-NMR (400 MHz, DMSO-d_6): δ (ppm) = 8.44 (s, 4H, N–C*H*–N), 3.93 (s, 16H, C$H_{2(backbone)}$/C$H_{2,(bridge)}$), 3.72 (s, 16H, C$H_{2,(bridge)}$/C$H_{2,(backbone)}$). ^{1}H-NMR (400 MHz, CD_3CN): δ (ppm) = 7.98–7.82 (m, 4H, N–C*H*–N), 4.00–3.82 (m, 16H, C$H_{2,(backbone)}$/C$H_{2,(bridge)}$), 3.73–3.65

© 2024 The Author(s). Published by the Royal Society of Chemistry

Open Access Article. Published on 27 March 2024. Downloaded on 4/30/2026 5:07:08 AM. This article is licensed under a Creative Commons Attribution 3.0 Unported Licence.

(m, 16H, $CH_{2,(bridge)}$/$CH_{2,(backbone)}$). ^{19}F-NMR (376 MHz, CD_3CN): δ (ppm) = −72.45 (d, $^1J_{P-F}$ = 713 Hz, PF_6^-). ESI-MS: m/z = calc. for $[\mathbf{H_4L6}–PF_6^-]^+$: 823.20 ($[M–PF_6^-]^+$); found: 822.94; calc. for $[\mathbf{H_4L6}\text{-}2PF_6^-]^+$: 339.11 ($[\mathbf{H_4L6}\text{-}2PF_6^-]^+$); found: 339.12.

Calix[4](–Et–Et–)imidazoliumtrifluoromethanesulfonate (H_4L8). 7 (1.00 g, 6.17 mmol, 2.00 eq.) is dissolved in dry MeCN (1.5 L), cooled to −30 °C and a solution of **4** (2.02 g, 6.20 mmol, 2.01 eq.) in dry MeCN (100 mL) is added dropwise over 5 h. After the addition, the reaction mixture is stirred for 72 h at ambient temperature. All volatile compounds are removed *in vacuo* and the resulting crude material is washed eight times with cold acetone (10 mL, 5 mL, 5 mL, 3 mL, 3 mL, 2 mL, 2 mL, 1 mL) and dried subsequently *in vacuo*. Without further purification, the titled compound **H_4L8** is obtained as a white solid (1.50 g, 1.54 mmol, 50%). ^{1}H-NMR (400 MHz, CD_3CN) δ (ppm) = 8.57 (t, ^4J = 1.6 Hz, 4H, N–C*H*–N), 7.39 (d, ^4J = 1.7 Hz, 8H, C*H*), 4.71 (s, 16H, CH_2). ^{13}C-NMR (101 MHz, CD_3CN) δ (ppm) = 138.49 (N–*C*H–N), 124.49 (H*C*=*C*H), 121.80 (q, $^1J_{19F-13C}$ = 320 Hz, OTf^-), 50.14 (CH_2–CH_2). ^{19}F-NMR (376 MHz, CD_3CN) δ (ppm) = −79.32 (CF_3). ^{1}H-NMR (400 MHz, DMSO-d_6) δ (ppm) = 9.00 (t, ^4J = 1.7 Hz, 4H, N–C*H*–N), 7.57 (d, ^4J = 1.6 Hz, 8H, C*H*), 4.74 (s, 16H, CH_2). ^{13}C-NMR (101 MHz, DMSO-d_6) δ (ppm) = 137.08 (N–*C*H–N), 123.28 (H*C*=*C*H), 120.66 (q, $^1J_{19F-13C}$ = 320 Hz, OTf^-), 49.24 (CH_2–CH_2). Elemental analysis for $C_{24}H_{28}N_8O_{12}F_{12}S_4$ (%) anal. calc.: C 29.54; H 2.84; N 11.54; S 13.13 found: C 29.54; H 2.84; N 11.54; S 13.25. ESI-MS: m/z $[\mathbf{H_4L8}–4OTf^-]^{4+}$ calc.: 95.06, found: 94.91, $[\mathbf{H_4L8}–3OTf^-]^{3+}$ calc.: 176.39, found 176.36, $[\mathbf{H_4L8}–2OTf^-]^{2+}$ calc.: 339.07, found: 339.22, $[\mathbf{H_4L8}–1OTf^-]^{1+}$ calc.: 827.03, found 826.93.

Calix[4](–Et–Et–)imidazoliumhexafluorophosphate (H_4L9). **H_4L8** (3.20 g, 3.28 mmol, 1.00 eq.) is dissolved in H_2O (300 mL) and added to a solution of NH_4PF_6 (3.20 g, 19.66 mmol, 6.00 eq.) in H_2O (50 mL). The resulting white precipitate is collected, washed three times with H_2O (10 mL, 7 mL, 5 mL) and dried subsequently *in vacuo*. Without further purification, the titled compound **H_4L9** is obtained as a white solid (2.80 g, 2.85 mmol, 88%). ^{1}H-NMR (400 MHz, CD_3CN) δ (ppm) = 8.44 (t, ^4J = 1.6 Hz, 4H, N–C*H*–N), 7.33 (d, ^4J = 1.7 Hz, 8H, C*H*), 4.70 (s, 16H, CH_2). ^{19}F-NMR (376 MHz, CD_3CN) δ (ppm) = −72.30 (d, $^1J_{FP}$ = 713 Hz, PF_6^-). ^{1}H-NMR (400 MHz, DMSO-d_6) δ (ppm) = 9.00 (s, 4H, N–C*H*–N), 7.55 (d, ^4J = 1.6 Hz, 8H, C*H*), 4.73 (s, 16H, CH_2). ^{13}C-NMR (101 MHz, DMSO-d_6) δ (ppm) = 137.26 (N–*C*H–N), 123.49 (H*C*=*C*H), 49.44 (CH_2–CH_2). Elemental analysis for $C_{20}H_{28}N_8F_{24}P_4$ (%) anal. calc.: C 25.01; H 2.94; N 11.67; S 0.00 found: C 25.08; H 2.90; N 11.31; S 0.00.

Pd[$C^{Et}C_{imi}(Me)_2C^{Et}C_{imi}(Me)_2$]hexafluorophosphate (PdL3). Ag_2O (150 mg, 648 μmol, 1.05 eq.) is added to a solution of **H_2L3** (300 mg, 617 μmol, 1.00 eq.) and NaOAc (202 mg, 2.47 mmol, 4.00 eq.) in dry MeCN (15 mL) and stirred for 1 h at ambient temperature, followed by the addition of $Pd(OAc)_2$ (145 mg, 648 μmol, 1.05 eq.). The resulting reaction mixture is heated to 80 °C for 3 d. After cooling to ambient temperature, the reaction mixture is filtered over a short plug of basic aluminum oxide. The filter column is eluted with MeCN (20 mL) and all volatile compounds are removed *in vacuo*. The resulting crude material is resuspended in MeCN (5 mL) and centrifuged. Upon the addition of Et_2O (20 mL) to the supernatant, a white solid is precipitated. The crude material is collected *via* centrifugation, washed with Et_2O (3 × 5 mL), redissolved in MeCN (5 mL) and precipitated with Et_2O (15 mL). After drying *in vacuo*, the titled compound **PdL3** is obtained as an off-white solid (140 mg, 178 μmol, 29%). Single crystals suitable for SC-XRD were obtained by slow diffusion of Et_2O into MeCN solution of **PdL3**. ^{1}H-NMR (400 MHz, CD_3CN) δ (ppm) = 4.32–4.22 (m, 4H, $CH_{2(backbone)}$), 3.71–3.51 (m, 20H, CH_2–CH_2, $CH_{2(backbone)}$), 2.97 (s, 12H, CH_3). ^{13}C-NMR (101 MHz, CD_3CN) δ (ppm) = 195.6 (N–*C*–N), 51.72 ($C_{(bridge)}$, $C_{(backbone)}$), 51.26 ($C_{(bridge)}$, $C_{(backbone)}$), 46.5 (CH_2), 37.62 (CH_3). ^{19}F-NMR (376 MHz, CD_3CN): δ (ppm) = −72.94 (d, $^1J_{P-F}$ = 706 Hz, PF_6). ^{1}H-NMR (400 MHz, DMSO-d_6) δ (ppm) = 4.35–4.13 (m, 4H, $CH_{2(backbone)}$), 3.82–3.57 (m, 20H, CH_2–CH_2, $CH_{2(backbone)}$), 2.95 (s, 12H, CH_3). ^{13}C-NMR (101 MHz, DMSO-d_6) δ (ppm) = 194.29 (N–*C*–N), 50.94 ($C_{(bridge)}$, $C_{(backbone)}$), 50.56 ($C_{(bridge)}$, $C_{(backbone)}$), 45.76 (CH_2), 37.17 (CH_3). Elemental analysis: for $C_{20}H_{36}F_{24}N_8P_4Pd_1$ (%) anal. calc.: C: 30.60, H: 4.62, N: 14.28, found: C: 30.93, H: 4.55, N: 14.14, S: 0.00. HR-ESI-MS: m/z $[\mathbf{PdL3}\text{-}2PF_6^-]^{2+}$ calc.: 247.1044, found: 247.1039, $[\mathbf{PdL3}–PF_6^-]^+$ calc.: 639.1735, found: 639.1720.

Pt[$C^{Et}C_{imi}(Me)_2C^{Et}C_{imi}(Me)_2$]hexafluorophosphate (PtL3). Ag_2O (150 mg, 648 μmol, 1.05 eq.) is added to a solution of **H_2L3** (300 mg, 617 μmol, 1.00 eq.) and NaOAc (202 mg, 2.47 mmol, 4.00 eq.) in dry MeCN (15 mL) and stirred for 1 h at ambient temperature, followed by the addition of $PtCl_2$ (145 mg, 648 μmol, 1.05 eq.). The resulting reaction mixture is heated to 80 °C for 3 d. After cooling to ambient temperature, the reaction mixture is filtered over a short plug of basic aluminum oxide. The filter column is eluted with MeCN (20 mL) and all volatile compounds are removed *in vacuo*. The resulting crude material is resuspended in MeCN (5 mL) and centrifuged. Upon the addition of Et_2O (20 mL) to the supernatant, a white solid is precipitated. The crude material is collected *via* centrifugation, washed with Et_2O (3 × 5 mL) and redissolved in MeCN (5 mL) and precipitated with Et_2O (15 mL). After drying *in vacuo*, the titled compound **PtL3** is obtained as an off-white solid (23 mg, 26 μmol, 4%). Single crystals suitable for SC-XRD were obtained by slow diffusion of Et_2O into MeCN solution of **PtL3**. Note; a clean EA could not be obtained, and the NMR includes impurities. ^{1}H-NMR (400 MHz, CD_3CN) δ (ppm) = 4.35–4.26 (m, 4H, $CH_{2(backbone)}$), 3.72–3.51 (m, 20H, CH_2–CH_2, $CH_{2(backbone)}$), 2.94 (s, 12H, CH_3). ^{13}C-NMR (101 MHz, CD_3CN) δ (ppm) = 188.38 (N–*C*–N), 51.47 (d, $C_{(bridge)}$, $C_{(backbone)}$), 46.39 (CH_2), 37.44 (CH_3).

Pd[($cC^{Et}CC^{Et}C_{imi}$)OTf] (PdL5). Ag_2O (155 mg, 670 μmol, 2.20 eq.) is added to a solution of **H_4L5** (300 mg, 305 μmol, 1.00 eq.) and NaOAc (200 mg, 2.42 mmol, 8.00 eq.) in dry MeCN/DMSO (12 mL 1 : 1) and stirred for 1 h at ambient temperature, followed by the addition of $Pd(OAc)_2$ (71.8 mg, 320 μmol, 1.05 eq.). The resulting reaction mixture is heated to 80 °C for 3 d and is filtered, after cooling to ambient temperature, over a short plug of basic aluminum oxide. The filter column is eluted with MeCN (100 mL) and all volatile compounds are removed *in vacuo*. The resulting oily solution (still approx. 6 mL of DMSO remaining) is resuspended in MeCN (6 mL) and centrifuged. Upon the addition of Et_2O (25 mL) to the supernatant, a brown/black solid is precipitated. After another addition of Et_2O (120 mL) a white

Open Access Article. Published on 27 March 2024. Downloaded on 4/30/2026 5:07:08 AM. This article is licensed under a Creative Commons Attribution 3.0 Unported Licence.

solid is precipitated. The white crude material is collected *via* centrifugation, washed with Et_2O (3 × 5 mL) and redissolved in MeCN (5 mL). After purification [3 times dissolving in MeCN (4 mL) and precipitating with Et_2O (∼15 mL)] and removing all volatile compounds *in vacuo*, the titled compound **PdL5** is obtained as an off-white solid (7.00 mg, 8.87 μmol, 3%). ^{1}H-NMR (400 MHz, CD_3CN): δ (ppm) = 4.10–4.00 (m, 8H, C$H_{2,(bridge)}$), 3.76–3.54 (m, 16H, C$H_{2,(backbone)}$), 3.52–3.45 (m, 8H, C$H_{2,(bridge)}$). ^{13}C-NMR (101 MHz, CD_3CN): δ (ppm) = 191.3 (N–*C*–N), 51.0 (*C*$H_{2,(bridge)}$/*C*$H_{2,(backbone)}$), 47.4 (*C*$H_{2,(backbone)}$/*C*$H_{2,(bridge)}$). ^{19}F-NMR (376 MHz, CD_3CN): δ (ppm) = −79.33 (CF_3). ESI-MS: *m*/*z* = calc. for [**PdL5**–OTf$^-$]$^+$: 639.13 ([**PdL5**–OTf$^-$]$^+$); found: 639.44; calc. for [**PdL5**–2OTf$^-$]$^+$: 245.09 ([M–2OTf$^-$]$^+$); found: 245.20.

Pd[(cC^{Et}CC^{Et}C$_{imi}$)PF$_6$] (PdL6). PdL6 is synthesized analog to **PdL5**; by converting **H$_4$L6** (230 mg, 238 μmol, 1.00 eq.) with Ag_2O (121 mg, 522 μmol, 2.20 eq.) in dry MeCN (4 mL) while stirring for 1 h at ambient temperature, followed by the addition of NaOAc (156 mg, 1.90 mmol, 8.00 eq.), $Pd(OAc)_2$ (56.0 mg, 249 μmol, 1.05 eq.) and is heated at 75 °C for 4 d. After purification [3 times dissolving in MeCN (4 mL) and precipitating with Et_2O (∼15 mL)] and removing all volatile compounds, **PdL6** is obtained as a pale-yellow solid (85.0 mg, 109 μmol, 46%). ^{1}H-NMR (400 MHz, CD_3CN): δ (ppm) = 4.13–4.02 (m, 8H, C$H_{2,(bridge)}$), 3.78–3.60 (m, 16H, C$H_{2,(backbone)}$), 3.52–3.46 (m, 8H, C$H_{2,(bridge)}$). ^{19}F-NMR (376 MHz, CD_3CN): δ (ppm) = −72.78 (d, $^1J_{P31-F19}$ = 707 Hz, PF_6) elemental analysis for $C_{20}H_{32}F_{12}N_8P_2Pd$ (%) anal. calc.: C 30.76; H 4.13; N 14.13; found: C 29.50; H 4.07; N 14.35. ESI-MS: *m*/*z* = calc. for [**PdL6**–PF$_6^-$]$^+$: 635.14 ([M–PF$_6^-$]$^+$); found: 635.21. HR-ESI-MS: *m*/*z* [**PdL6**–2PF$_6^-$]$^{2+}$ calc.: 245.0887, found: 245.0890, [**PdL6** + H_2O–2PF$_6^-$]$^{2+}$ calc.: 254.0940, found: 254.0944, [**PdL6**–PF$_6^-$]$^+$ calc.: 635.1422, found: 635.1425, [**PdL6** + H_2O–PF$_6^-$]$^+$ calc.: 653.1527, found: 653.1534.

Pd[(cC^{Et}CC^{Et}C)OTf] (PdL8). Ag_2O (74.7 mg, 322 μmol, 1.05 eq.) is added to a solution of **H$_4$L8** (320 mg, 307 μmol, 1.00 eq.) and NaOAc (202 mg, 2.46 mmol, 4.00 eq.) in dry MeCN (15 mL) and stirred for 1 h at ambient temperature, followed by the addition of $Pd(OAc)_2$ (72.4 mg, 322 μmol, 1.05 eq.). The resulting reaction mixture is heated to 80 °C for 4 d. After cooling to ambient temperature, the reaction mixture is filtered over a short plug of basic aluminum oxide. The filter column is eluted with MeCN (50 mL) and all volatile compounds are removed *in vacuo*. The resulting crude material is resuspended in MeCN (5 mL) and centrifuged. Upon the addition of Et_2O (20 mL) to the supernatant, a white solid is precipitated. The crude material is collected *via* centrifugation, washed with Et_2O (3 × 5 mL) and redissolved in MeCN (5 mL). After the precipitation with Et_2O (15 mL) and drying *in vacuo*, the titled compound **PdL8** is obtained as an off-white solid (119 mg, 153 μmol, 50%). ^{1}H-NMR (400 MHz, CD_3CN) δ (ppm) = 7.20 (s, 8H, C*H*), 5.02–4.93 (m, 8H, CH_2), 4.47–4.39 (m, 8H, CH_2). ^{13}C-NMR (101 MHz, CD_3CN) δ (ppm) = 165.84 (N–*C*–N), 123.77 (*C*H), 49.11 (s, *C*H_2–*C*H_2). ^{1}H-NMR (400 MHz, DMSO-d$_6$) δ (ppm) = 7.52 (s, 8H, C*H*), 5.05–4.95 (m, 8H, CH_2), 4.52–4.42 (m, 8H, CH_2). ^{13}C-NMR (101 MHz, DMSO-d$_6$) δ (ppm) = 163.80 (N–*C*–N), 123.32 (*C*H), 48.14 (*C*H_2–*C*H_2). Elemental analysis for $C_{20}H_{28}N_8F_{24}P_4$ + 1 MeCN (%) anal. calc.: C 35.07; H 3.31; N 15.33; S 7.80 found: C 35.26; H 3.21; N 15.73; S 7.82. HR-ESI-MS: *m*/*z* [**PdL8**–2OTf$^-$]$^{2+}$ calc.: 241.0574, found: 241.0570, [**PdL8**–OTf$^-$]$^+$ calc.: 631.0674, found: 631.0658.

Pd[(cC^{Et}CC^{Et}C)PF$_6$] (PdL9). PdL8 (95 mg, 122 μmol, 1.00 eq.) is dissolved in H_2O (35 mL), after the addition of NH_4PF_6 (50.0 mg, 305 μmol, 2.5 eq.) a white precipitate is collected *via* centrifuge and washed three times with H_2O (5 mL, 3 mL, 3 mL) and Et_2O (10 mL, 5 mL, 3 mL). After drying *in vacuo*, the titled compound **PdL9** is obtained as an off-white solid (39 mg, 50 μmol, 41%). Single crystals suitable for SC-XRD were obtained by slow diffusion of Et_2O into MeCN solution of **PdL8**. ^{1}H-NMR (400 MHz, CD_3CN) δ (ppm) = 7.22 (s, 8H, C*H*), 4.97 (m, 8H, CH_2), 4.43 (m, 8H, CH_2). ^{19}F-NMR (376 MHz, CD_3CN) δ (ppm) = −72.93 (d, $^1J_{FP}$ = 713 Hz, PF$_6^-$). HR-ESI-MS: *m*/*z* [**PdL9**–2PF$_6^-$]$^{2+}$ calc.: 241.0574, found: 241.0570, [**PdL9**–PF$_6^-$]$^+$ calc.: 627.0796, found: 627.0782.

Pt[(cC^{Et}CC^{Et}C)OTf] (PtL8). Ag_2O (209 mg, 900 μmol, 2.20 eq.) is added to a solution of **H$_4$L8** (400 mg, 410 μmol, 1.00 eq.) and NaOAc (202 mg, 2.46 mmol, 4.00 eq.) in dry MeCN (30 mL) and stirred for 1 h at ambient temperature, followed by the addition of $Pt(MeCN)_2Cl_2$ (156 mg, 450 μmol, 1.10 eq.). The resulting reaction mixture is heated to 80 °C for 3 d and is filtered, after cooling to ambient temperature, over a short plug of basic aluminum oxide. The filter column is eluted with MeCN (50 mL) and all volatile compounds are removed *in vacuo*. The resulting crude material is resuspended in MeCN (5 mL) and centrifuged. Upon the addition of Et_2O (20 mL) to the supernatant, a white solid is precipitated. The crude material is collected *via* centrifugation, washed with Et_2O (3 × 5 mL) and redissolved in MeCN (5 mL). After the precipitation with Et_2O (15 mL) and drying *in vacuo*, the titled compound **PtL8** is obtained as an off-white solid (90 mg, 103 μmol, 25%).^{1}H-NMR (400 MHz, CD_3CN) δ (ppm) = 7.19 (s, 8H, C*H*), 5.11–4.94 (m, 8H, CH_2), 4.50–4.38 (m, 8H, CH_2). ^{1}H-NMR (400 MHz, DMSO-d$_6$) δ (ppm) = 7.49 (s, 8H, C*H*), 5.06–4.97 (m, 8H, CH_2), 4.54–4.44 (m, 8H, CH_2). ^{13}C-NMR (101 MHz, CD_3CN) δ (ppm) = 159.39 (N–*C*H–N), 123.58 (H*C*=*C*H), 48.86 (*C*H_2–*C*H_2). ^{19}F-NMR (376 MHz, CD_3CN) δ (ppm) = −79.27 (CF_3). HR-ESI-MS: *m*/*z* [**PtL8**–2OTf$^-$]$^{2+}$ calc.: 285.5881, found: 285.5864, [**PtL8**–OTf$^-$]$^+$ calc.: 720.1287, found: 720.1264.

Au[(cC^{Et}CC^{Et}C)PF$_6$] (AuL9). H$_4$L8 (500 mg, 458 μmol, 1.00 eq.), $KAuCl_4 \times 2H_2O$ (209 mg, 505 μmol, 1.05 eq.), and NaOAc (197 mg, 2.41 mmol, 5.00 eq.) are suspended in dry DMSO (5 mL). The resulting reaction mixture is stirred for 5 h at 100 °C and filtered at ambient temperature. MeCN (5 mL) is added to the filtrate. After the addition of Et_2O (30 mL) to the solution, white solid precipitated. It is washed with MeCN (3 × 5 mL) and DCM (2 × 5 mL) and after the removal of all volatiles *in vacuo*, the solid is dissolved in H_2O (2 mL) and added dropwise to a solution of NH_4PF_6 (353 mg, 2.17 mmol, 4.00 eq.) in H_2O (5 mL). The resulting white precipitate is collected and washed with H_2O (3 × 5 mL) and after removal of all volatiles *in vacuo*, the titled compound **AuL9** (230 mg, 228 mmol, 47%) is obtained as a white solid. ^{1}H-NMR (400 MHz, CD_3CN) δ (ppm) = 7.47 (s, 8H, C*H*), 4.89–4.77 (m, 8H, CH_2), 4.76–4.66 (m, 8H, CH_2). ^{13}C-NMR (101 MHz, CD_3CN) δ (ppm) = 146.03 (N–*C*H–N), 125.92 (H*C*=*C*H), 48.58 (*C*H_2–*C*H_2). Elemental analysis for $C_{20}H_{24}AuF_{18}N_8P_3 \times 0.1$ MeCN (%) anal. calc.: C 24.62; H 2.70; N 11.11;

© 2024 The Author(s). Published by the Royal Society of Chemistry

S 0.00 found: C 24.82; H 2.78; N 11.15; S 0.57. HR-ESI-MS: *m*/*z* [**AuL9**–3PF_6^-]$^{3+}$ calc.: 191.0591, found: 191.0587, [**AuL9**–PF_6^-]$^+$ calc.: 863.1068, found: 863.1038.

Conflicts of interest

There are no conflicts to declare.

Acknowledgements

All authors thank Prof. Dr T. Simon (University Cologne) for providing the SK-N-AS cell line, Dr Seeger for providing the Nalm-6 cell line. A. Prokop thanks the Dr. Kleist Foundation (Berlin), Foundation David (Cologne), Koch Foundation (Berlin) and Blankenheimerdorf e.V. (Eifel) for the financial support in the biological studies. Further thanks go to A. Gradenegger, F. Tschernuth from Prof. Dr S. Inoue, and C. Hoefer for synthetic support of the compound **H_4L8** and Patrick Mollik for HR-ESI-MS measurements. Thanks also go to Rea Sangiovanni for the graphical abstract.

Notes and references

1 A. J. Arduengo, R. L. Harlow and M. Kline, *J. Am. Chem. Soc.*, 1991, **113**, 361–363, DOI: **10.1021/ja00001a054**.
2 P. Bellotti, M. Koy, M. N. Hopkinson and F. Glorius, *Nat. Rev. Chem*, 2021, **5**, 711–725, DOI: **10.1038/s41570-021-00321-1**.
3 T. P. Schlachta and F. E. Kühn, *Chem. Soc. Rev.*, 2023, **52**, 2238–2277, DOI: **10.1039/D2CS01064J**.
4 A. Biffis, M. Baron and C. Tubaro, in *Adv. Organomet. Chem.*, ed. P. J. Pérez, Academic Press, 2015, vol. 63, pp. 203–288, DOI: **10.1016/bs.adomc.2015.02.002**.
5 V. Charra, P. de Frémont and P. Braunstein, *Coord. Chem. Rev.*, 2017, **341**, 53–176, DOI: **10.1016/j.ccr.2017.03.007**.
6 M. A. Bernd, E. B. Bauer, J. Oberkofler, A. Bauer, R. M. Reich and F. E. Kühn, *Dalton Trans.*, 2020, **49**, 14106–14114, DOI: **10.1039/D0DT02598D**.
7 E. B. Bauer, M. A. Bernd, M. Schütz, J. Oberkofler, A. Pöthig, R. M. Reich and F. E. Kühn, *Dalton Trans.*, 2019, **48**, 16615–16625, DOI: **10.1039/C9DT03183A**.
8 J. F. Schlagintweit, C. H. G. Jakob, K. Meighen-Berger, T. F. Gronauer, A. Weigert Muñoz, V. Weiß, M. J. Feige, S. A. Sieber, J. D. G. Correia and F. E. Kühn, *Dalton Trans.*, 2021, **50**, 2158–2166, DOI: **10.1039/D0DT04114A**.
9 C. H. G. Jakob, B. Dominelli, J. F. Schlagintweit, P. J. Fischer, F. Schuderer, R. M. Reich, F. Marques, J. D. G. Correia and F. E. Kühn, *Chem.–Asian J.*, 2020, **15**, 4275–4279, DOI: **10.1002/asia.202001104**.
10 M. R. Anneser, S. Haslinger, A. Pöthig, M. Cokoja, J.-M. Basset and F. E. Kühn, *Inorg. Chem.*, 2015, **54**, 3797–3804, DOI: **10.1021/ic503043h**.
11 G. Moreno-Alcántar, P. Picchetti and A. Casini, *Angew. Chem., Int. Ed.*, 2023, **62**, e202218000, DOI: **10.1002/anie.202218000**.
12 M. Mora, M. C. Gimeno and R. Visbal, *Chem. Soc. Rev.*, 2019, **48**, 447–462, DOI: **10.1039/C8CS00570B**.
13 M. G. Karaaslan, A. Aktaş, C. Gürses, Y. Gök and B. Ateş, *Bioorg. Chem.*, 2020, **95**, 103552, DOI: **10.1016/j.bioorg.2019.103552**.
14 L. Oehninger, R. Rubbiani and I. Ott, *Dalton Trans.*, 2013, **42**, 3269–3284, DOI: **10.1039/C2DT32617E**.
15 I. Ott, in *Inorganic and Organometallic Transition Metal Complexes with Biological Molecules and Living Cells*, ed. K. K.-W. Lo, Academic Press, 2017, pp. 147–179, DOI: **10.1016/B978-0-12-803814-7.00005-8**.
16 I. Ott, in *Adv. Inorg. Chem.*, ed. P. J. Sadler and R. van Eldik, Academic Press, 2020, vol. 75, pp. 121–148, DOI: **10.1016/bs.adioch.2019.10.008**.
17 S. Nayak and S. L. Gaonkar, *ChemMedChem*, 2021, **16**, 1360–1390, DOI: **10.1002/cmdc.202000836**.
18 Nature Editorial, *Nature*, 2023, **617**, 438, DOI: **10.1038/d41586-023-01612-x**.
19 C. Heinemann, T. Müller, Y. Apeloig and H. Schwarz, *J. Am. Chem. Soc.*, 1996, **118**, 2023–2038, DOI: **10.1021/ja9523294**.
20 M. N. Hopkinson, C. Richter, M. Schedler and F. Glorius, *Nature*, 2014, **510**, 485–496, DOI: **10.1038/nature13384**.
21 T. P. Schlachta, Master's thesis, Technical University of Munich, Garching, Germany, 2020.
22 M. Scholl, S. Ding, C. W. Lee and R. H. Grubbs, *Org. Lett.*, 1999, **1**, 953–956, DOI: **10.1021/ol990909q**.
23 P. S. Athey and G. E. Kiefer, *J. Org. Chem.*, 2002, **67**, 4081–4085, DOI: **10.1021/jo016111d**.
24 Y. Chun, N. J. Singh, I. C. Hwang, J. W. Lee, S. U. Yu and K. S. Kim, *Nat. Commun.*, 2013, **4**, 1797, DOI: **10.1038/ncomms2758**.
25 Z. Li, E. R. R. Mackie, P. Ramkissoon, J. C. Mather, N. Wiratpruk, T. P. Soares da Costa and P. J. Barnard, *Dalton Trans.*, 2020, **49**, 12820–12834, DOI: **10.1039/D0DT02225J**.
26 J. W. Emsley, J. Feeney and L. H. Sutcliffe, *High Resolution Nuclear Magnetic Resonance Spectroscopy*, Elsevier, 2013, vol. 2.
27 R. J. Abraham, M. Canton and L. Griffiths, *Magn. Reson. Chem.*, 2001, **39**, 421–431.
28 P. de Frémont, N. Marion and S. P. Nolan, *Coord. Chem. Rev.*, 2009, **253**, 862–892, DOI: **10.1016/j.ccr.2008.05.018**.
29 H. V. Huynh, *Chem. Rev.*, 2018, **118**, 9457–9492, DOI: **10.1021/acs.chemrev.8b00067**.
30 T. P. Schlachta, G. G. Zámbó, M. J. Sauer, I. Rüter, C. A. Hoefer, S. Demeshko, F. Meyer and F. E. Kühn, *J. Catal.*, 2023, **426**, 234–246, DOI: **10.1016/j.jcat.2023.07.018**.
31 W. A. Herrmann, G. Gerstberger and M. Spiegler, *Organometallics*, 1997, **16**, 2209–2212.
32 P. De Fremont, N. Marion and S. P. Nolan, *Coord. Chem. Rev.*, 2009, **253**, 862–892.
33 J. F. Schlagintweit, L. Nguyen, F. Dyckhoff, F. Kaiser, R. M. Reich and F. E. Kühn, *Dalton Trans.*, 2019, **48**, 14820–14828.
34 P. J. Altmann, D. T. Weiss, C. Jandl and F. E. Kühn, *Chem.–Asian J.*, 2016, **11**, 1597–1605, DOI: **10.1002/asia.201600198**.
35 B. Dominelli, G. M. Roberts, C. Jandl, P. J. Fischer, R. M. Reich, A. Pöthig, J. D. G. Correia and F. E. Kühn, *Dalton Trans.*, 2019, **48**, 14036–14043, DOI: **10.1039/C9DT03035B**.
36 M. M. Watts, *J. Am. Oil Chem. Soc.*, 1990, **67**, 993–995.

Open Access Article. Published on 27 March 2024. Downloaded on 4/30/2026 5:07:08 AM. This article is licensed under a Creative Commons Attribution 3.0 Unported Licence.

Open Access Article. Published on 27 March 2024. Downloaded on 4/30/2026 5:07:08 AM. This article is licensed under a Creative Commons Attribution 3.0 Unported Licence.

37 M. A. Kalam, K. Haraguchi, S. Chandani, E. L. Loechler, M. Moriya, M. M. Greenberg and A. K. Basu, *Nucleic Acids Res.*, 2006, **34**, 2305–2315, DOI: **10.1093/nar/gkl099**.
38 C.-Y. Liao, K.-T. Chan, C.-Y. Tu, Y.-W. Chang, C.-H. Hu and H. M. Lee, *Chem.–Eur. J.*, 2009, **15**, 405–417, DOI: **10.1002/chem.200801296**.
39 W. A. Herrmann, M. Elison, J. Fischer, C. Köcher and G. R. J. Artus, *Angew Chem. Int. Ed. Engl.*, 1995, **34**, 2371–2374, DOI: **10.1002/anie.199523711**.
40 D. T. Weiss, P. J. Altmann, S. Haslinger, C. Jandl, A. Pöthig, M. Cokoja and F. E. Kühn, *Dalton Trans.*, 2015, **44**, 18329–18339, DOI: **10.1039/C5DT02386F**.
41 R. Dorta, E. D. Stevens, N. M. Scott, C. Costabile, L. Cavallo, C. D. Hoff and S. P. Nolan, *J. Am. Chem. Soc.*, 2005, **127**, 2485–2495, DOI: **10.1021/ja0438821**.
42 M. Süßner and H. Plenio, *Chem. Commun.*, 2005, 5417–5419, DOI: **10.1039/B512008J**.
43 F. E. Hahn, V. Langenhahn, T. Lügger, T. Pape and D. Le Van, *Angew. Chem., Int. Ed.*, 2005, **44**, 3759–3763, DOI: **10.1002/anie.200462690**.
44 R. McKie, J. A. Murphy, S. R. Park, M. D. Spicer and S.-z. Zhou, *Angew. Chem., Int. Ed.*, 2007, **46**, 6525–6528, DOI: **10.1002/anie.200702138**.
45 Z. Lu, S. A. Cramer and D. M. Jenkins, *Chem. Sci.*, 2012, **3**, 3081–3087, DOI: **10.1039/C2SC20628E**.
46 C. S. t. Brinke and F. Ekkehardt Hahn, *Dalton Trans.*, 2015, **44**, 14315–14322, DOI: **10.1039/C5DT02115D**.
47 H. M. Bass, S. A. Cramer, A. S. McCullough, K. J. Bernstein, C. R. Murdock and D. M. Jenkins, *Organometallics*, 2013, **32**, 2160–2167, DOI: **10.1021/om400043z**.
48 H. V. Huynh, Y. Han, R. Jothibasu and J. A. Yang, *Organometallics*, 2009, **28**, 5395–5404, DOI: **10.1021/om900667d**.
49 P. J. Altmann and A. Pöthig, *Chem. Commun.*, 2016, **52**, 9089–9092, DOI: **10.1039/C6CC00507A**.
50 H. M. Bass, S. A. Cramer, J. L. Price and D. M. Jenkins, *Organometallics*, 2010, **29**, 3235–3238, DOI: **10.1021/om100625g**.
51 E. B. Bauer, M. A. Bernd, M. Schütz, J. Oberkofler, A. Pöthig, R. M. Reich and F. E. Kühn, *Dalton Trans.*, 2019, **48**, 16615–16625.
52 It needs to be noted that the elemental analysis still includes MeCN as an impurity.
53 F. K.-M. Chan, K. Moriwaki and M. J. De Rosa, in *Immune Homeostasis: Methods and Protocols*, ed. A. L. Snow and M. J. Lenardo, Humana Press, Totowa, NJ, 2013, pp. 65–70, DOI: **10.1007/978-1-62703-290-2_7**.
54 S. Dasari and P. B. Tchounwou, *Eur. J. Pharmacol.*, 2014, **740**, 364–378, DOI: **10.1016/j.ejphar.2014.07.025**.
55 N. Vasan, J. Baselga and D. M. Hyman, *Nature*, 2019, **575**, 299–309, DOI: **10.1038/s41586-019-1730-1**.
56 J. F. Schlagintweit, C. H. G. Jakob, N. L. Wilke, M. Ahrweiler, C. Frias, J. Frias, M. König, E.-M. H. J. Esslinger, F. Marques, J. F. Machado, R. M. Reich, T. S. Morais, J. D. G. Correia, A. Prokop and F. E. Kühn, *J. Med. Chem.*, 2021, **64**, 15747–15757, DOI: **10.1021/acs.jmedchem.1c01021**.
57 A. Frost and A. Carlson, *J. Org. Chem.*, 1959, **24**, 1581–1582, DOI: **10.1021/jo01092a614**.
58 D. E. Goldberg and K. C. Patel, *J. Inorg. Nucl. Chem.*, 1972, **34**, 3583–3584, DOI: **10.1016/0022-1902(72)80260-4**.
59 L. W. Jenneskens, J. Mahy, E. M. M. de Brabander-van den Berg, I. van der Hoef and J. Lugtenburg, *Recl. Trav. Chim. Pays-Bas*, 1995, **114**, 97–102, DOI: **10.1002/recl.19951140305**.
60 E. Lindner, G. von Au and H. J. Eberle, *Chem. Ber.*, 1981, **114**, 810–813.
61 Z. Li, E. R. Mackie, P. Ramkissoon, J. C. Mather, N. Wiratpruk, T. P. S. da Costa and P. J. Barnard, *Dalton Trans.*, 2020, **49**, 12820–12834.
62 G. R. Fulmer, A. J. M. Miller, N. H. Sherden, H. E. Gottlieb, A. Nudelman, B. M. Stoltz, J. E. Bercaw and K. I. Goldberg, *Organometallics*, 2010, **29**, 2176–2179, DOI: **10.1021/om100106e**.

© 2024 The Author(s). Published by the Royal Society of Chemistry